THE ASTROPHYSICAL JOURNAL, 445:211–220, 1995 May 20

DEEP INFRARED ARRAY PHOTOMETRY OF GLOBULAR CLUSTERS. III. M13

T. J. DAVIDGE[1]
Gemini Canada Project Office, Dominion Astrophysical Observatory, 5071 West Saanich Road, Victoria, B.C. Canada V8X 4M6; and
Department of Geophysics and Astronomy, University of British Columbia; davidge@dao.nrc.ca

AND

W. E. HARRIS[1]
Department of Physics and Astronomy, McMaster University, Hamilton, Ontario, Canada L8S 4M1;
harris@physun.physics.mcmaster.ca
Received 1994 August 11; accepted 1994 November 30

ABSTRACT

We have used the California-France-Hawaii Telescope (CFHT) REDEYE infrared camera to obtain deep J and K' images of four fields in the globular cluster M13. The composite (K, $J-K$) color-magnitude diagram (CMD) extends from the upper red giant branch (RGB) to 2 mag below the main-sequence turnoff (MSTO). Selected [Fe/H] ~ -1.6 isochrones from Bergbusch & VandenBerg (1992) and Straniero & Chieffi (1991) are transformed onto the near-infrared observational plane, and these suggest an age for M13 in the range 14–16 Gyr. We emphasize that any effort to estimate ages should be considered as tentative given uncertainties in the input physics; however, these uncertainties notwithstanding, comparisons between the near-infrared isochrones indicate that age *differences* of order ± 2 Gyr should be detectable among metal-poor clusters on the (K, $J-K$) plane. Building on this result, we find that the difference in $J-K$ color between the MSTO and the base of the RGB in M13 is the same as in M4, and we conclude that these clusters have similar ages. This conclusion is verified by comparing (1) the K brightnesses of the MSTO and (2) the morphologies of optical CMDs. Finally, we investigate the mass function of main-sequence stars in M13 with distances between 3 and 6 core radii from the cluster center. The mass functions in the interval 0.55 and 0.8 $M_\odot$ are relatively flat, independent of radius. Optical studies at larger radii have found nonzero mass function indices in this same mass interval, and we attribute this radial variation in mass function morphology to dynamical evolution.

Subject headings: globular clusters: individual (M13) — infrared: stars — stars: evolution — stars: luminosity function, mass function

1. INTRODUCTION

Because it is among the closest globular clusters, and is located at a moderately high Galactic latitude, M13 has been the target of several photometric studies. Early photographic and photoelectric investigations by Kadla et al. (1976), Sandage (1970), Baum et al. (1959), Savedoff (1956), Arp (1955), Arp & Johnson (1955), and Baum (1954) defined the cluster color-magnitude diagram (CMD) from the upper red giant branch (RGB) to well below the main-sequence turnoff (MSTO). More recent CCD studies by Richer & Fahlman (1986) and Lupton & Gunn (1986) have traced the cluster sequence to $V \sim 24$, which corresponds to stars with masses near 0.2 $M_\odot$.

Although there is a wealth of optical photometric data, only a small number of stars in M13 have been observed at wavelengths longward of 1 μm. Cohen, Frogel, & Persson (1978) obtained aperture measurements of 14 bright giants, and these data were used as part of a larger effort to calibrate giant branch properties as a function of metallicity (Frogel, Cohen, & Persson 1983a). More recently, Buckley & Longmore (1992) obtained K photometry of a small number of main-sequence stars and, after combining these data with optical measurements, estimated basic properties for M13 such as temperature of the MSTO and distance. The absence of a larger set of near-infrared measurements is unfortunate since, by virtue of the extensive optical photometric database, coupled with the broad agreement which exists between the various spectroscopic metallicity estimates (§ 4), M13 is an ideal calibrator for near-infrared isochrones. The issue of isochrone calibration longward of 1 μm is important, as efforts to transform theoretical isochrones onto the near-infrared observational plane using bolometric corrections and color calibrations predicted by model atmospheres have revealed surface gravity and temperature-dependent errors, which distort the transformed models (e.g., Davidge & Simons 1994a, b, hereafter Papers I and II; Ferraro et al. 1994).

Aside from studies of CMD morphology, deep infrared photometry can also be used to derive mass functions independent of those computed at optical wavelengths. The mass function of M13 is of particular interest since studies by Richer & Fahlman (1986), Lupton & Gunn (1986), Drukier et al. (1988) and Richer et al. (1990) suggest that at low masses the M13 mass function may be steeper than in the solar neighborhood. Consequently, M13 should play in important role in defining correlations between mass function index and quantities such as metallicity and distance from the Galactic center (e.g., Djorgovski, Piotto, & Capaccioli 1993). The study of the M13 mass function is also significant since star counts suggest that the mass function of halo field stars may follow that of clusters (Reid & Majewski 1993).

M13 should also prove to be an excellent comparison object for metal-poor clusters in the Galactic bulge which, according to some models of spiral galaxy formation (e.g., Larson 1990), may be the oldest in the Galaxy. Indeed, VandenBerg, Bolte, &

[1] Visiting Astronomer, Canada-France-Hawaii Telescope, which is operated by the National Research Council of Canada, the Centre National de la Recherche Scientifique de France, and the University of Hawaii.

Stetson (1990) included M13 in their sample of [Fe/H] ~ -1.6 halo clusters for relative age determinations and, based on the Richer & Fahlman (1986) photometry, suggested that M13 may be the oldest cluster in this group, although the lack of a large database of subgiant branch (SGB) and lower RGB stars with CCD photometry prevented definitive conclusions from being drawn. Near-infrared photometry is required for studies of Galactic bulge clusters, as these objects are often heavily reddened, and spatial variation in the distribution of obscuring material smears optical CMDs. Fortunately, these effects are greatly reduced at wavelengths longward of 1 μm, and (K, $J-K$) CMDs should prove useful for probing age differences. In future papers of this series, we will compare our M13 CMD with those of Galactic bulge clusters.

In the current paper, we discuss J and K' observations of four fields in M13. The main goals of this study are (1) to define the (K, $J-K$) CMD of M13 over a wide range of brightnesses, (2) to compare the CMD with evolutionary models, and (3) to investigate the cluster mass function. The observations and reductions are described in § 2, while details of the photometry and the resulting (K, $J-K$) CMD are discussed in § 3. In § 4 we compare the CMD with theoretical isochrones, which have been translated onto the near-infrared observational plane using a technique that relies on color relations defined by metal-poor subdwarfs and giants, combined with synthetic photometry predicted from model atmospheres. We investigate the mass function of M13 in § 5, and we conclude with a brief summary in § 6.

2. OBSERVATIONS AND REDUCTION

The data were recorded during the nights of UT August 28, 29, and 31 1993 using the Canada-France-Hawaii Telescope (CFHT) REDEYE camera, which was mounted at the f/8 focus of the telescope. The camera contains a Rockwell 256 × 256 Hg:Cd:Te array with 40 μm square pixels; a detailed description of the instrument has been given by Simons et al. (1993). The data were recorded through the narrow-field optics, so that the image scale is 0.″2 pixel^{-1} and each exposure samples a field 51″ on a side. Because of the high background levels inherent to broadband near-infrared observations, multiple exposures were recorded of each field, and the telescope was offset a few arcseconds between these (i.e., "dithering") to facilitate the identification and suppression of bad pixels. Consequently, the final co-added images cover regions slightly less than 51″ on a side.

Four cluster fields were observed through a Caltech-CTIO J and a K' (Wainscoat & Cowie 1992) filter. The coordinates of each field, as well as the integration times and image quality in the final frames, are summarized in Table 1. A number of standard stars from the list compiled by Casali & Hawarden (1992) were also observed, and these data will be discussed further in § 3.

A problem developed with the array controller while the Field 3 data were being recorded, such that the read noise in one quadrant became very high. This had a significant impact on photometry of faint sources, so this portion of each Field 3 image was excluded from the final analysis. However, the photometric performance of the other quadrants was unaffected.

The data were reduced using procedures similar to those described in Papers I and II. A median dark frame was subtracted from each image, and the results were divided by normalized sky flats, constructed on a nightly basis from all deep integrations recorded on that night. The flat-fielded images were sky subtracted, aligned, median combined, and then trimmed to the area common to all exposures. The final J images are shown in Figure 1.

TABLE 1

SUMMARY OF OBSERVATIONS

Field	R.A. (1950.0)	Decl. (1950.0)	R_{center}[a] (Core Radii)	Exposures (s)	FWHM
1.....	16^{h}39^{m}54^s.4	+36°33′31″.5	0.4	3 × 10(J)	0″.5
				3 × 10(K')	0.5
2.....	16 40 01.1	+36 36 06.1	3.9	3 × 90(J)	0.5
				3 × 90(K')	0.5
3.....	16 39 32.	+36 31 01.0	5.9	20 × 180(J)	0.6
				20 × 180(K')	0.6
4.....	16 39 40.2	+36 33 59.5	3.4	50 × 60(J)	0.6
				45 × 60(K')	0.6

[a] Distance from cluster center, assuming core radius = 49″.9 (Webbink 1985).

3. PHOTOMETRIC MEASUREMENTS AND THE (K, $J-K$) DIAGRAM

3.1. *Photometric Measurements*

The brightnesses of standard stars were measured using the aperture photometry routine PHOT, which is part of the DAOPHOT (Stetson 1987) photometry package. Aperture sizes were determined by inspecting radial intensity profiles of the various standard stars. Linear transformations of the form

$$M = m + \psi_M C + \mu_M X + \zeta_M$$

were then fitted to the measurements using the method of least squares. Here, M and m are the standard and instrumental magnitudes, C is the instrumental color, X is the airmass, ψ_M and ζ_M are the transformation coefficients, and μ_M is the extinction coefficient. The instrumental K' measurements were transformed into K values.

The extinction coefficients in J and K are relatively small and require a large number of standard stars to be reliably determined. A total of 20 standard star observations were made during the course of the five night observing run. Because of this modest sample size, it was decided to adopt the Mauna Kea J and K extinction coefficients computed by Guarnieri, Dixon, & Longmore (1991). After fixing the extinction coefficients at these values, a least-squares fit to the transformation relations revealed ($j-k'$) color coefficients of 0.015 ± 0.037 and 0.020 ± 0.056 for J and K, respectively. The uncertainties in the derived zero points are $\sim$0.01 mag. A list of the standards which were observed and the residuals from the fitted transformation relations, in the sense standard value minus computed value, is given in Table 2.

Photometry of cluster stars was performed with the PSF-fitting routine ALLSTAR (Stetson & Harris 1988). Artificial star experiments were run to determine completeness fractions and assess systematic errors in the measured brightnesses for each field. Typically 30–50 artificial stars per 0.5 mag interval were added to the various frames, and this was done over the course of several runs to prevent artificially raising the degree of crowding. The completeness curves for Fields 1 and 3, which have the shortest and longest integration times, are compared in Figure 2.

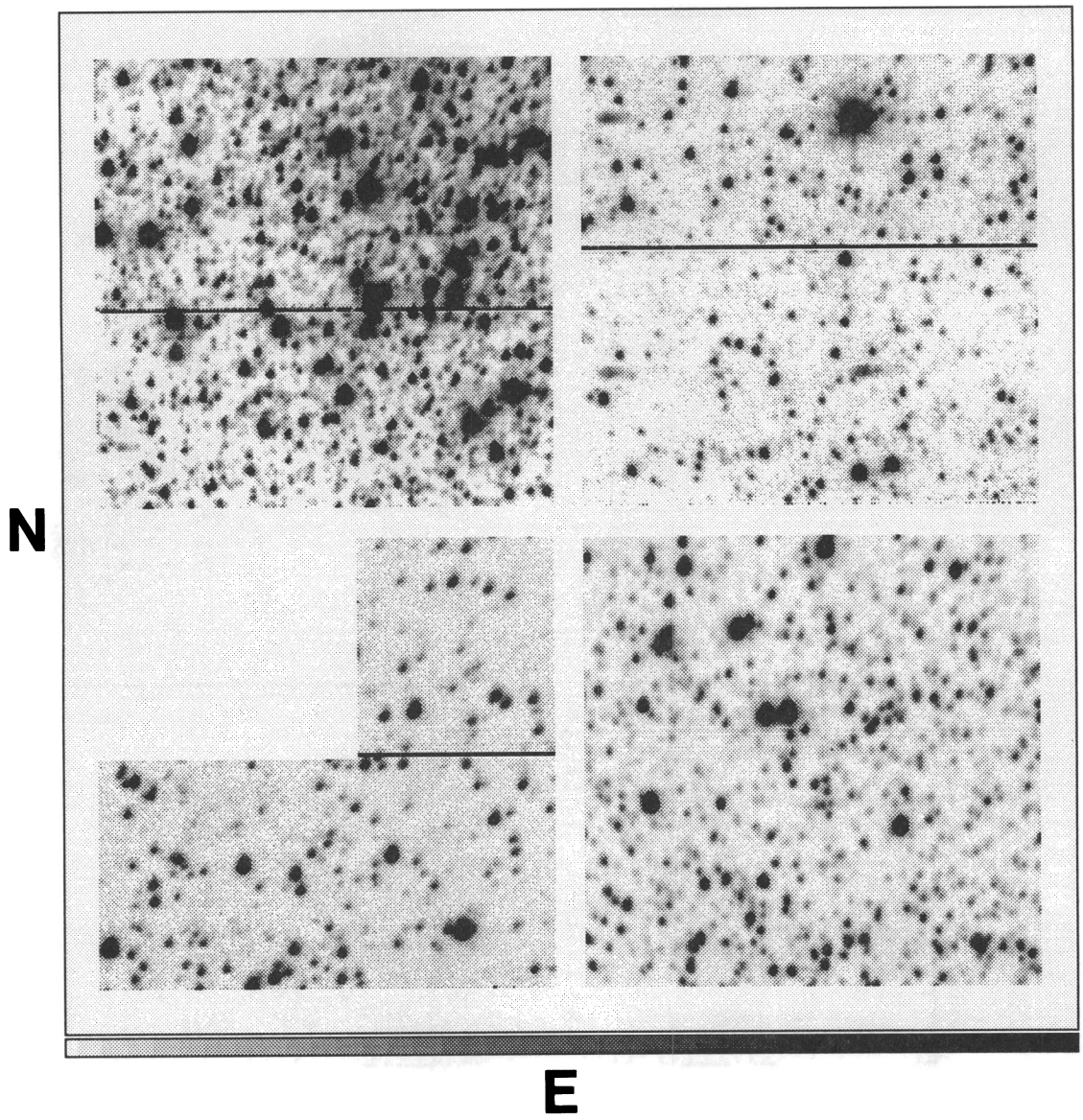

FIG. 1.—Final J images for Fields 1 (*upper left-hand corner*), 2 (*upper right-hand corner*), 3 (*lower left-hand corner*), and 4 (*lower right-hand corner*). In all cases north is to the left, and east is at the bottom. The blank area in the Field 3 observations is due to a bad quadrant on the detector.

3.2. *The* $(K, J-K)$ *CMD of M13*

The $(K, J-K)$ diagrams for all four fields are shown in Figure 3. Only those stars with uncertainties in the computed brightnesses due to errors in the PSF-fit, as calculated by ALLSTAR, ≤ 0.07 mag in each filter are plotted. Initial comparisons revealed that the loci of the Field 1 and 4 CMDs agreed to within 0.02 mag; however, the CMDs for Fields 2 and 3 were offset by ~ 0.07 mag in $J-K$ from the Field 1 and 4 data, in the sense that the Field 2 data were too red, whereas the Field 3 data were too blue. We are unable to offer an unambiguous explanation for these offsets, although the standard star data provide a clue to the likely cause, which we now discuss. The data for Fields 1, 2, and 3 were recorded largely on the night of August 28. Based on the data in Table 2, the standard deviation in $\Delta_{JK} = \Delta_J - \Delta_K$ among the standard stars observed on this night is ± 0.07 mag, which is remarkably (and probably fortuitously!) similar to the observed field-to-field scatter in the color calibration. For comparison, the Field 4 data were recorded exclusively on the night of August 31, and the standard deviation in Δ_{JK} for the standard stars observed on this night is only 0.03 mag. This comparison of the standard star data suggests that modest changes in sky transparency may be responsible for the offsets in color calibration. To compensate for these, the Field 2 and 3 data were shifted to match those of Fields 1 and 4, and it is the corrected measurements for Fields 2 and 3 which are shown in Figure 3.

An independent check of our color calibration is highly desirable given the field-to-field variation noted in the preceding paragraph. To facilitate such a check, normal points were created from the data in Figure 3 by sorting the observations into bins of width ± 0.25 mag in K and then calculating the mean of the $J-K$ distribution in each bin after applying sequential 2 σ rejections. The Field 1 data were used to define the cluster sequence above the MSTO, while the Field 2, 3, and 4 data were used for the SGB and main sequence. The results are listed in Table 3. Also shown in Table 3 are the estimated

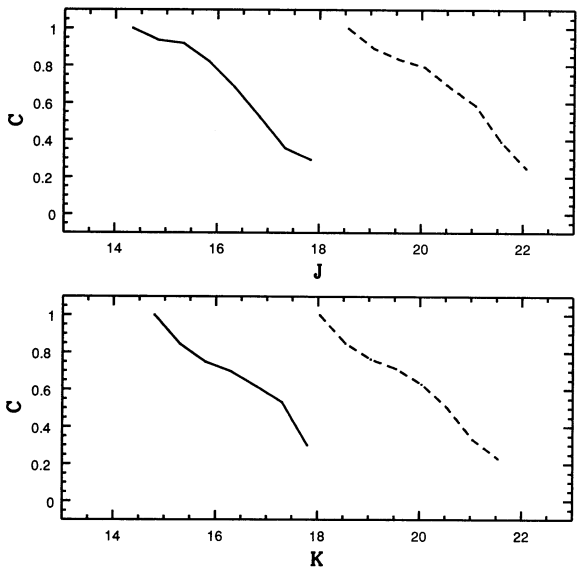

FIG. 2.—*J* (*top panel*) and *K* (*bottom panel*) completeness curves for Fields 1 (*solid line*) and 3 (*dashed line*).

TABLE 2

STANDARD STAR RESIDUALS

Date (1993)	Star[a]	J	K'	Δ_J	Δ_K
Aug 28.....	23	12.997	12.374	+0.030	−0.024
	27	13.494	13.123	+0.017	−0.054
	34	12.819	12.989	−0.064	−0.067
	30	11.923	12.015	−0.074	+0.062
Aug 29.....	24	10.904	10.753	−0.008	−0.076
	25	10.231	9.756	+0.045	+0.085
	29	13.175	13.346	−0.018	+0.036
	2	10.713	10.466	+0.008	−0.021
	4	10.556	10.264	−0.007	+0.001
Aug 30.....	24	10.904	10.753	−0.011	−0.011
	23	12.997	12.374	−0.044	−0.104
	27	13.494	13.123	+0.021	−0.058
	30	11.923	12.015	+0.043	+0.043
	32	13.459	13.664	+0.051	+0.047
	7	11.105	10.940	−0.029	+0.087
Aug 31.....	29	13.175	13.346	−0.008	+0.005
	6	13.239	13.374	+0.001	−0.046
	2	10.713	10.466	+0.039	+0.069
	4	10.556	10.264	+0.042	+0.017
Sep 1.....	35	12.231	11.757	−0.039	+0.003

[a] FS number listed by Casali & Hawarden 1992.

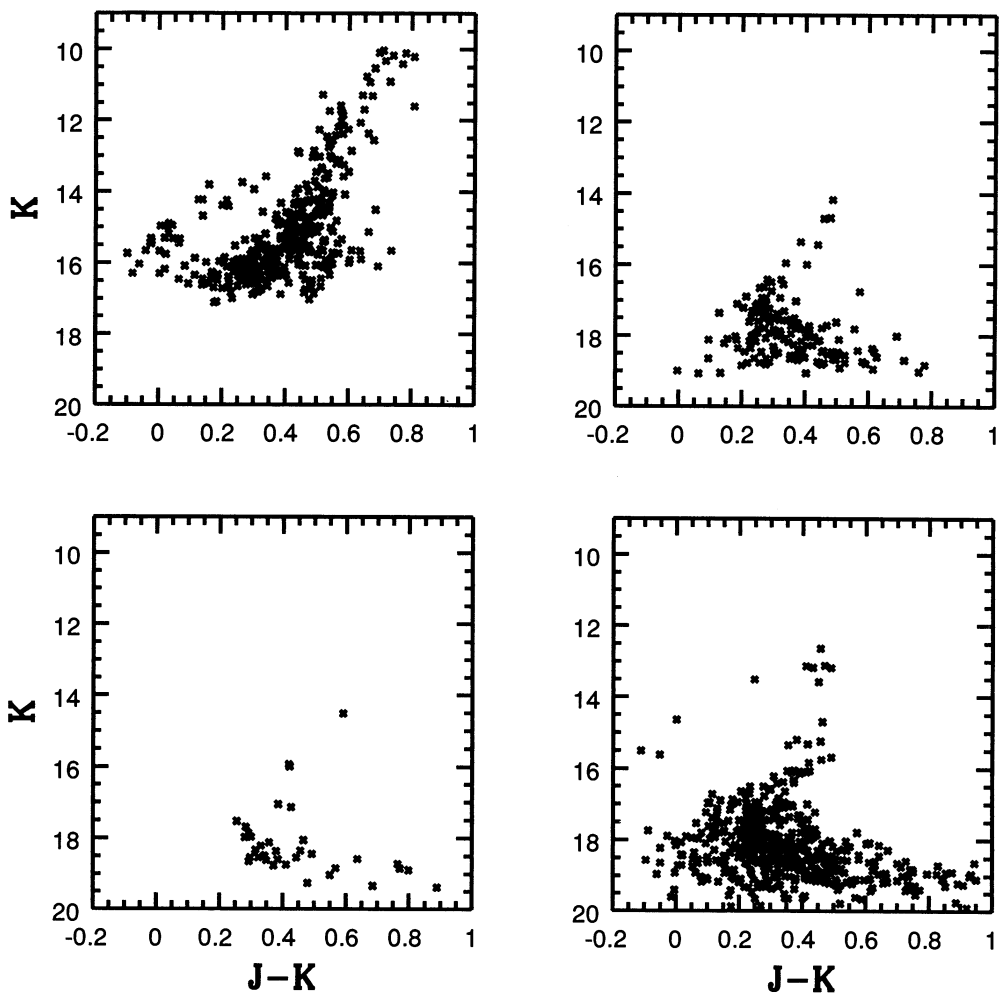

FIG. 3.—(K, $J-K$) CMDs for Fields 1 (*upper left-hand corner*), 2 (*upper right-hand corner*), 3 (*lower left-hand corner*), and 4 (*lower right-hand corner*). Only those stars with uncertainties in either magnitude of 0.07 mag or less, as derived by ALLSTAR, have been plotted.

TABLE 3

M13 NORMAL POINTS

K	$J-K$
10.0.....	0.75 ± 0.02
10.5.....	0.72 ± 0.02
11.0.....	0.68 ± 0.02
11.5.....	0.62 ± 0.02
12.0.....	0.59 ± 0.02
12.5.....	0.57 ± 0.02
13.0.....	0.55 ± 0.01
13.5.....	0.52 ± 0.01
14.0.....	0.50 ± 0.01
14.5.....	0.47 ± 0.01
15.0.....	0.44 ± 0.01
15.5.....	0.43 ± 0.02
16.0.....	0.36 ± 0.02
16.5.....	0.31 ± 0.02
17.0.....	0.27 ± 0.02
17.5.....	0.29 ± 0.02
18.0.....	0.32 ± 0.02
18.5.....	0.39 ± 0.02
19.0.....	0.54 ± 0.07

uncertainties in the normal points, which are the standard errors of the mean computed from the $J-K$ distribution in each brightness bin following the sequential rejection iterations described above. We emphasize that these uncertainties are internal and that additional systematic uncertainties in the calibration amounting to ~0.01–0.02 mag are also present.

In Figure 4 the normal points are compared with the aperture measurements made by Cohen et al. (1978) and the ridgeline predicted from the measurements made by Buckley & Longmore (1992). Buckley & Longmore obtained K, but not J, measurements and computed $V-K$ colors from existing optical photometry. In order to create measurements which could be compared with our data, $J-K$ colors were calculated using the $(J-K, V-K)$ calibration for metal-poor subdwarfs derived in § 4. It is evident from Figure 4 that both the Cohen et al. and the Buckley & Longmore data are in good agreement with our observations, adding confidence to our color calibration.

How does the near-infrared CMD of M13 compare with those of other metal-poor clusters? The ridgeline of the [Fe/H] = −1.3 (Zinn & West 1984) cluster M4, taken from Paper I and shifted to match the color and brightness of the M13 sequence in the vicinity of the MSTO, is compared with our normal points in Figure 4. Considering the uncertainties in the M13 normal points, there is reasonable agreement between the two sequences in the vicinity of the MSTO, and the color of the base of the RGB in the two clusters is identical, suggesting similar ages. If M4 and M13 are coeval, then their MSTO brightnesses should also be similar, although a comparison of this nature is complicated by uncertainties in reddening and differences in metallicity. The near-infrared CMD of M4 presented in Paper I indicates that $K_{\rm MSTO} \sim 14.25$, while in M13 $K_{\rm MSTO} \sim 17.0$, with estimated uncertainties of ±0.10 mag. Based on data given in Table 4 of Armandroff (1989), $E(B-V) = 0.40$ and $V_{\rm HB} = 13.35$ for M4, while $E(B-V) = 0.02$ and $V_{\rm HB} = 14.95$ for M13. Adopting the RR Lyrae brightness calibration predicted by Lee, Demarque, & Zinn (1990) and the reddening curve tabulated by Rieke & Lebofsky (1985), such that $A_K = 0.112A_V$ and $E(J-K) = 0.52E(B-V)$, then $M_K^{\rm MSTO} = 2.60$ in M4 and 2.65 in M13. Theoretical near-infrared isochrones constructed using

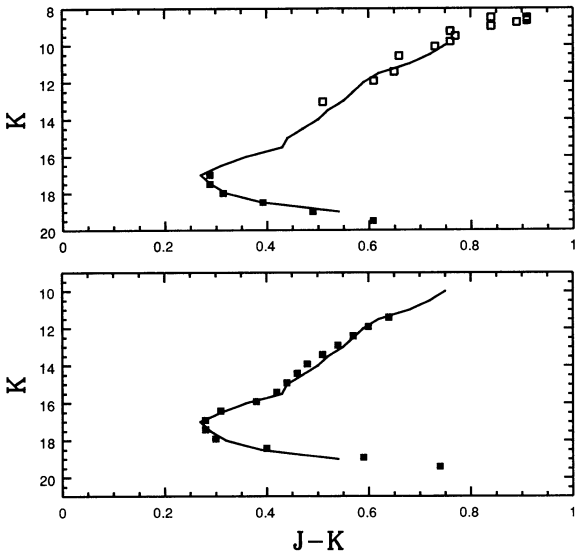

FIG. 4.—Comparisons between the M13 normal point sequence (*solid curve*) and other data sets. In the top panel the observations made by Cohen et al. (1978) of bright M13 giants are shown as open squares, while the ridgeline defined from photometry of main-sequence stars by Buckley & Longmore (1992) is shown as filled squares. In the lower panel, the normal points for the cluster M4 by Davidge & Simons (1994a) are shown as solid squares. The M4 data have been shifted to match the color and brightness of the M13 MSTO.

the procedures described in § 4 predict that $\Delta M_K^{\rm MSTO}/\Delta t = 0.1$ mag Gyr^{-1} and $\Delta M_K^{\rm MSTO}/\Delta$[Fe/H] = 0.1 mag/[Fe/H] dex. Consequently, the near-infrared brightnesses of the MSTO are also consistent with similar ages for M4 and M13.

The hypothesis that M4 and M13 have similar ages can be tested further using optical data. To this end, we compared the M4 normal points derived by Alcaino, Liller, & Alvarado (1988) with those for M13 from Richer & Fahlman (1986), and

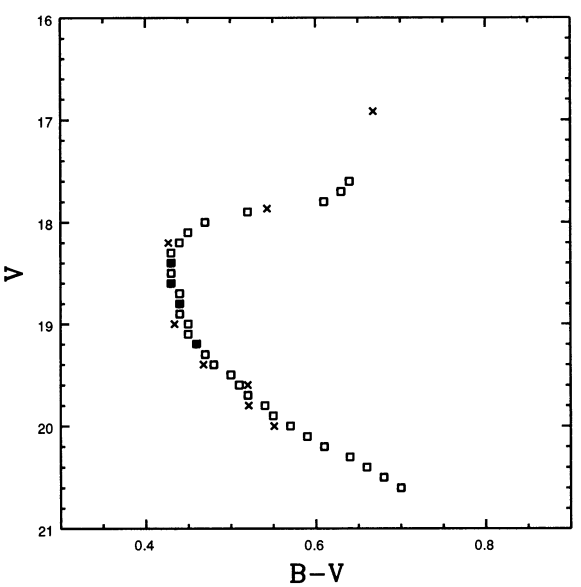

FIG. 5.—Comparison between M13 (*crosses*) and M4 (*open squares*) normal points, based on observations obtained by Richer & Fahlman (1986) and Alcaino et al. (1988), respectively. The two brightest M13 points were obtained by averaging the colors and brightnesses of the two SGB and three lower RGB stars observed by Richer & Fahlman (1986). The M4 data were shifted to match the color and brightness of the M13 MSTO.

the result is shown in Figure 5 where, as in Figure 4, the M4 data have been shifted to match the color and brightness of the M13 MSTO. Although the lower RGB is poorly defined in both clusters, there appears to be general agreement between the M4 and M13 sequences on the (V, $B-V$) plane. Clearly, additional optical observations covering the SGB and lower RGB will be required to confirm this result. Nevertheless, given that age differences of ± 2 Gyr should be detectable between metal-poor clusters in the (K, $J-K$) plane (§ 4), we tentatively conclude that M13 and M4 have similar ages. We note that a tacit assumption behind this conclusion is that the abundances of key atomc species, such as oxygen, do not vary among clusters with similar [Fe/H], since differences in chemical composition can mimic age effects on the CMD (VandenBerg & Stetson 1991).

4. COMPARISON WITH THEORETICAL MODELS

Before comparing the observations with theoretical sequences, we briefly review metallicity estimates for M13, with emphasis on spectroscopic studies. The main purpose of this exercise is to establish the mean metallicity of the cluster, so that this parameter can be fixed for comparisons with isochrones. Cohen (1978), Leep, Wallerstein, & Oke (1986), Wallerstein, Leep, & Oke (1987), and Lehnert, Bell, & Cohen (1991) obtained spectra of bright M13 giants and concluded that [Fe/H] lies between -1.5 and -1.6, with a mild preference for values at the lower end of this range. The sole discrepant spectroscopic study is that by Pilachowski, Wallerstein, & Leep (1980), who found [Fe/H] ~ -1.42 based on five giants. This result aside, the spectroscopic data are consistent with the mean metallicity computed by Zinn & West (1984), who used a variety of indicators to find [Fe/H] $= -1.65 \pm 0.06$. Consequently, in the following we will compare our observations with models having [Fe/H] ~ -1.6.

Although the photometric scatter in the optical CMD of M13 indicates that the star-to-star metallicity dispersion must be small (Folgheraiter, Penny, & Griffiths 1993), there is evidence for a range of CNO abundances, at least among the most evolved stars. This is potentially important when comparing observations with evolutionary models, as the abundances of species such as oxygen can influence isochrone morphology (e.g., VandenBerg & Stetson 1991). Suntzeff (1981) and Langer, Suntzeff, & Kraft (1992) found that giants in M13 show a range of CN strengths at a given $B-V$, with the majority being CN-strong. Leep et al. (1986), Brown, Wallerstein, & Oke (1991), and Kraft et al. (1992, 1993) find a range of oxygen abundances, although most of the M13 giants they studied appear to be oxygen-*deficient* (i.e., [O/Fe] ≤ 0). This is very different from what is seen among field giants and dwarfs (e.g., Abia & Rebolo 1989; Barbuy & Erdelyi-Mendes 1989); nevertheless, given the evolved nature of these stars, it is possible that the M13 studies may not be measuring primordial abundances but rather may be seeing the results of mixing. In the following, we will consider models which make different assumptions concerning [O/Fe].

In Papers I and II it was found that isochrones transformed onto the near-infrared observational plane using relations derived from model atmospheres contained luminosity-dependent calibration errors, which are largest in the vicinity of the MSTO. Bell (1992) was the first to detect these and suggested that uncertainties in the H^- free-free opacity may be partly responsible. Nevertheless, once corrected for calibration errors, certain sections of the transformed isochrones, such as the RGB, are able to closely reproduce the observations. In Paper II an effort was made to avoid calibration problems by constructing empirical color relations, which were in turn used to derive M_K and $J-K$ from the tabulated values of M_V and $B-V$. This procedure assumes that the optical isochrones do not contain large calibration errors, an assumption which appears to be valid (VandenBerg 1992). In fact, the near-infrared isochrones created in this manner provide a reasonable match to the observations, although a significant shortcoming is that there are some parts of the CMD, such as the base of the RGB, where the paucity of nearby calibrating stars makes it difficult to derive optical-infrared color relations. In the current paper, we describe a hybrid technique, which builds on the strengths of the theoretical and empirical calibration methods, to transform selected isochrones onto the near-infrared observational plane.

The first step is to assemble empirical color relations appropriate for [Fe/H] ~ -1.6. To this end, optical-infrared color relations were derived for very low mass stars, bright subdwarfs, and bright giants. The relations between $B-V$, $J-K$, and $V-K$ for halo subdwarfs from Table 6 of Leggett (1992) were adopted for stars near the bottom of the main sequence, while color relations for brighter subdwarfs were derived from data tabulated by Laird, Carney, & Latham (1988) for stars with [Fe/H] between -1.5 and -2.0. Color relations for bright giants were derived from the photometry tabulated by Cohen et al. (1978), Cohen & Frogel (1982), and Frogel, Persson, & Cohen (1983) for the clusters NGC 288, NGC 1904, NGC 2298, NGC 4372, NGC 4833, NGC 5024, NGC 5272, NGC 5286, NGC 5904, NGC 6254, NGC 6752, and NGC 7006 which, according to Zinn & West (1984), span a range of metallicities similar to that used for the bright subdwarfs. The data used to derive the bright subdwarf and giant color relations are summarized in Figures 6 ($B-V$ vs. $J-K$) and 7 ($B-V$ vs. $V-K$), while the adopted color relations are listed in Tables 4 and 5.

The color relations do not cover the SGB and lower RGB. These gaps were filled by extrapolating the empirical color relations using values of $\Delta(J-K)/\Delta(B-V)$ and $\Delta(V-K)/\Delta(B-V)$ derived from the synthetic photometry tabulated by Bell & Gustafsson (1989) and Bell (1992). We emphasize that

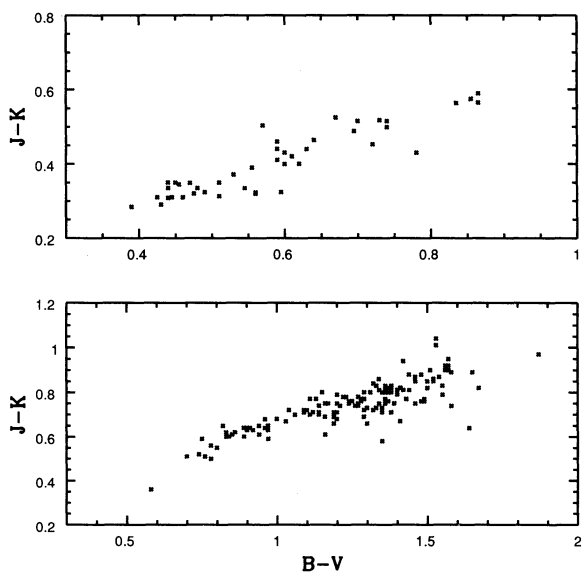

FIG. 6.—($B-V$, $J-K$) relations for dwarfs (*top panel*) and giants (*lower panel*). Note the different axial scales on the two panels.

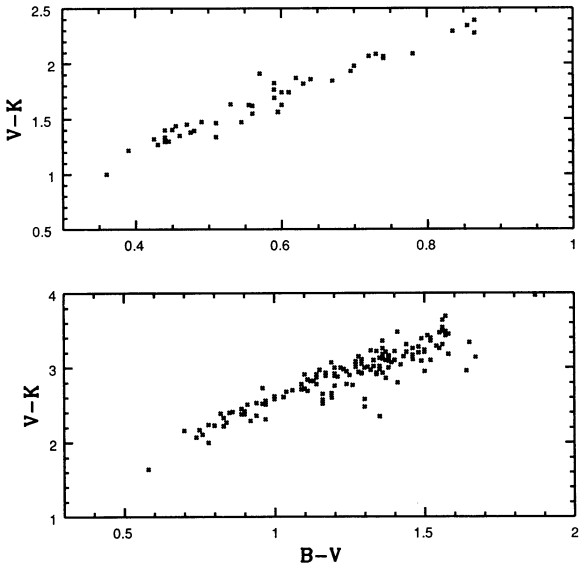

FIG. 7.—($B-V$, $V-K$) relations for dwarfs (*top panel*) and giants (*lower panel*). Note the different axial scales on the two panels.

although the synthetic photometry contains significant calibration errors, these data are nevertheless able to reproduce the *shape* of the RGB (e.g., Paper I), so they should provide reliable guides for extrapolation.

The procedures described above was used to transform selcted [Fe/H] ~ -1.6 isochrones from Bergbusch & VandenBerg (1992), who assume nonsolar oxygen abundances, and Straniero & Chieffi (1991), who assume [O/Fe] = 0, onto the near-infrared observational plane. The 12 and 16 Gyr Bergbusch & VandenBerg isochrones and 16 and 20 Gyr Straniero & Chieffi isochrones are compared in Figure 8. Age differences are most evident among the Bergsbusch & Vandenberg (1992)

TABLE 4

COLOR RELATIONS FOR SUBDWARFS

$B-V$	$J-K$	$V-K$
1.65	0.72	5.05
1.55	0.70	4.40
1.50	0.69	3.93
1.35	0.68	3.35
0.90	0.59	2.43
0.80	0.56	2.10
0.70	0.49	1.87
0.60	0.43	1.63
0.50	0.36	1.38
0.40	0.28	1.23

TABLE 5

COLOR RELATIONS FOR GIANTS

$B-V$	$J-K$	$V-K$
1.60	0.93	3.52
1.50	0.87	3.34
1.40	0.81	3.16
1.30	0.77	3.04
1.20	0.75	2.92
1.10	0.70	2.77
1.00	0.67	2.59
0.90	0.63	2.43
0.80	0.57	2.24
0.70	0.48	1.99

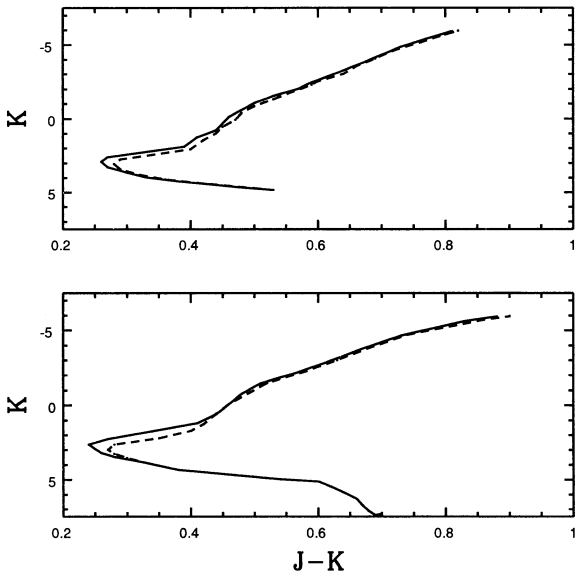

FIG. 8.—Near-infrared isochrones derived from the sequences tabulated by Straniero & Chieffi (1991; *top panel*) and Bergbusch & VandenBerg (1992; *lower panel*). The sequences in the top panel are for 16 (*solid line*) and 20 Gyr (*dashed line*), while the lower panel shows sequences with ages of 12 (*solid line*) and 16 Gyr (*dashed line*). It is readily evident that the ability to detect a given age difference depends on the cluster age.

isochrones, as these extend to the youngest ages. The Bergbusch & VandenBerg isochrones predict a change in the $J-K$ color of the MSTO of $\sim$0.05 mag between 12 and 16 Gyr, while the brightness of the SGB changes by $\sim$0.6 mag.

The theoretical sequences are compared with the M13 normal points in Figures 9 and 10, while the Straniero & Chieffi (1991) sequences are compared with actual data from Fields 2 and 3 in Figure 11. The placement of the models on these diagrams assumes $E(J-K) = 0.01$ and $\mu_0 = 14.29$, values which result if (1) $E(B-V) = 0.02$ and $V_{HB} = 14.95$ (Armandroff 1989); (2) $M_V^{HB} = 0.6$; and (3) $E(J-K) = 0.52E(B-V)$ (e.g., Rieke & Lebofsky 1985). Neither set of

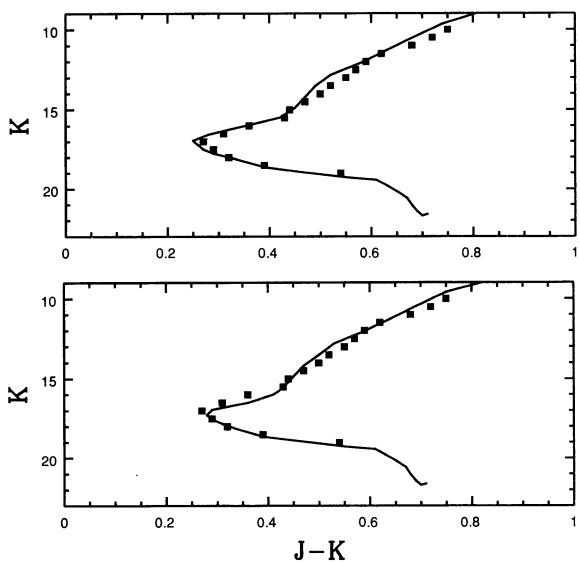

FIG. 9.—The M13 normal points (*solid squares*) compared with 12 Gyr (*top panel*) and 16 Gyr (*lower panel*) [Fe/H] ~ -1.6 isochrones from Bergbusch & VandenBerg (1992). See text for additional details.

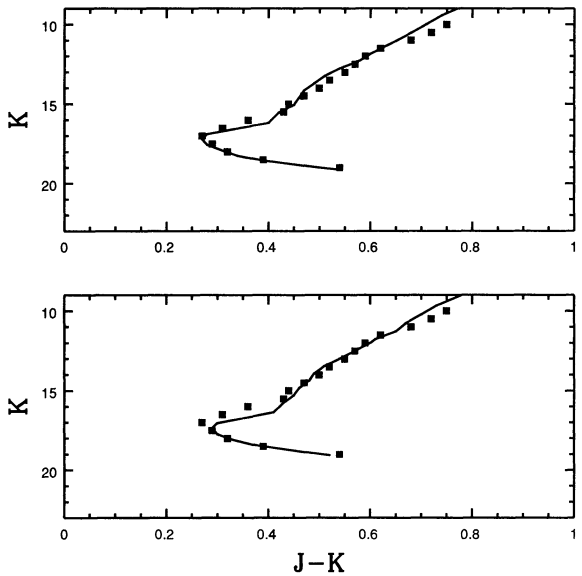

FIG. 10.—The M13 normal points (*solid squares*) compared with 16 Gyr (*top panel*) and 20 Gyr (*lower panel*) [Fe/H] ~ -1.6 isochrones from Straniero & Chieffi (1991). See text for additional details.

models provides an entirely satisfactory fit to the RGB; nevertheless, in both cases the isochones are able to match the main sequence fainter than $K \sim 18$. The exact age inferred for M13 depends on the models that are used, although it appears that models with ages in the range 14–16 Gyr should provide the best match to the color of the MSTO and should be able to reproduce the brightness difference between the SGB and MS at a fixed $J-K$. However, we emphasize that shortcomings in the input physics of stellar structure models make the determination of an absolute age uncertain. These uncertainties notwithstanding, it is evident from Figures 8, 9, 10, and 11 that the $(K, J-K)$ diagram could be used to detect age *differences* on the order of ± 2 Gyr among metal-poor clusters.

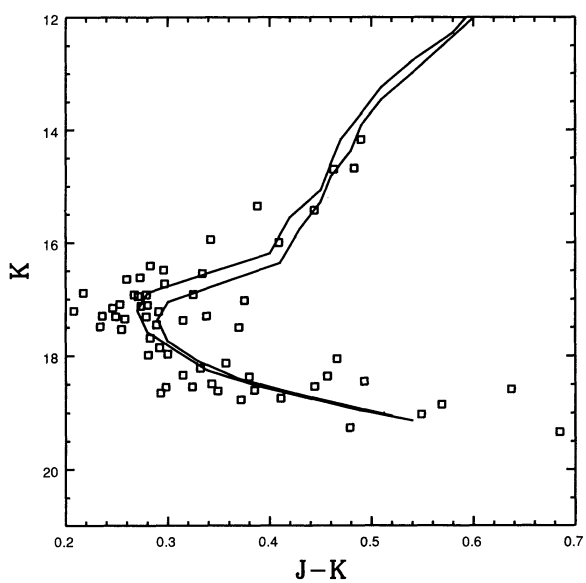

FIG. 11.—16 and 20 Gyr near-infrared isochrones derived from the sequences tabulated by Straniero & Chieffi (1991), compared with data from Fields 2 ($K < 17.5$) and 3 ($K > 17.5$).

5. LUMINOSITY AND MASS FUNCTIONS

Lupton & Gunn (1986), Drukier et al. (1988), and Richer et al. (1990) investigated the mass function of main-sequence stars in the outer regions of M13. These studies found that (1) the number of stars per mass interval increases with decreasing mass over all parts of the main sequence; (2) there are discontinuities in the mass function near 0.4–0.5 $M_\odot$, such that a single power law cannot fit the entire range of masses; and (3) at low masses the mass function is steeper than in the solar neighborhood.

The completeness-corrected K luminosity functions of main-sequence stars in Fields 2, 3, and 4 are shown in Figure 12, where N_K is the number of stars per 0.5 mag interval per square arcmin. The faint limit of the luminosity functions was set at $K \sim 19$, the point at which a coherent main sequence can no longer can be traced in Figure 3. The luminosity functions for Fields 2 and 4 are largely parallel; however, the Field 3 luminosity function appears to be steeper than the others.

A mass-luminosity relation derived from the near-infrared 16 Gyr Bergbusch & VandenBerg (1992) isochrone generated in § 4 was applied to the K luminosity functions to create mass functions, and the results are shown in Figure 13, where N_M refers to the number of stars per square arcminute per solar mass. The mass functions for Fields 2 and 4 appear to be very flat down to log $(M) \sim -0.2$ (i.e., $\sim 0.6\ M_\odot$). Although the Field 3 mass function appears to be tilted with respect to others, this finding rests largely on the most massive bins, where the uncertainties are large due to small number statistics.

In order to quantify the slopes of the mass functions, power laws of the form $N\,dM \propto M^x\,dM$ were fitted to the curves in Figure 13. The entire 0.60–0.78 $M_\odot$ range was included in these fits, and the results are listed in Table 6. The results in this table verify the visual appearance of Figure 13, in that the mass function exponents of Fields 2 and 4 are not significantly different from zero. For comparison, the mass functions

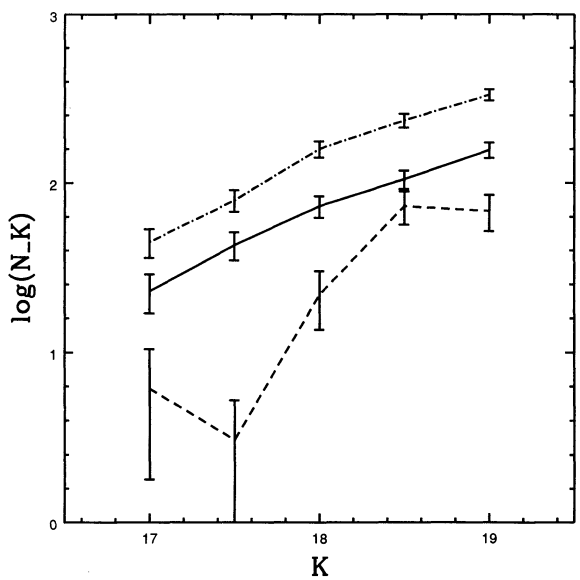

FIG. 12.—The completeness-corrected K luminosity functions for Fields 2 (*solid line*), 3 (*dashed line*), and 4 (*dashed-dotted line*). The error bars reflect counting statistics. N_K is the number of stars per square arcminute per 0.5 mag interval.

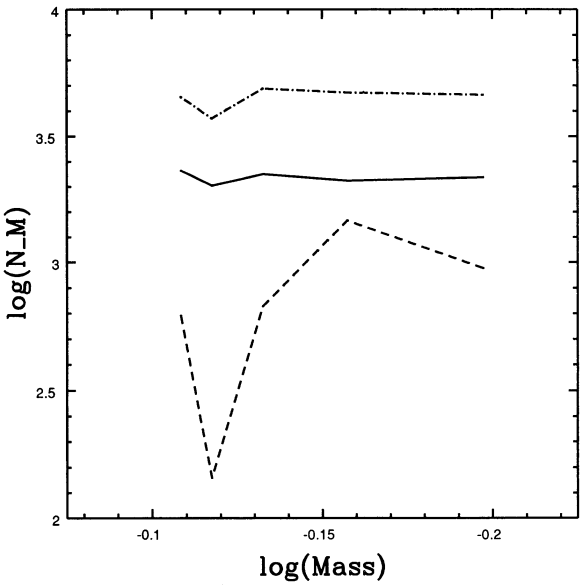

FIG. 13.—The mass functions for Fields 2 (*solid line*), 3 (*dashed line*), and 4 (*dashed-dotted line*). N_M is the number of stars per square arcminute per solar mass.

published by Lupton & Gunn (1986), Drukier et al. (1988), and Richer et al. (1990) at larger radii suggest that the mass function exponent in this same mass interval is significantly different from zero. This radial variation in mass function morphology is qualitatively consistent with dynamical evolution. Pryor, Smith, & McClure (1986) modeled mass segregation in globular clusters, and, if the concentration index for M13 is $C = 1.5$, as claimed by these authors, the mass function exponent between 3 and 6 core radii should change by ~ 0.5–1.0 if the primordial mass spectrum was like that in the solar neighborhood. It is apparent from the uncertainties listed in Table 6 that a change in mass function exponent of this size would go undetected with the current data set.

TABLE 6

MASS FUNCTION EXPONENTS

Field	R^a	x_{ms}
2	3.9	$+0.1 \pm 0.4$
3	5.9	-6.1 ± 5.0
4	3.4	-0.5 ± 0.7

[a] Distance from cluster center, in core radii, as presented in Table 1.

6. SUMMARY

The main conclusions of this paper are as follows:

1. The $(K, J-K)$ CMDs of M13 and M4 are very similar in the vicinity of the MSTO and lower RGB, suggesting that these clusters have comparable ages. This result is consistent with existing CCD data, although there is a need to better define the SGBs of these clusters at optical wavelengths.

2. Selected [Fe/H] ~ -1.6 isochrones from Bergsbusch & VandenBerg (1992) and Straniero & Chieffi (1991) have been transformed onto the near-infrared observational plane using a technique which relies on empirical color relations derived from metal-poor stars and synthetic photometry derived from model atmospheres. A comparison of near-infrared isochrones suggests that age differences of order ± 2 Gyr can be detected among metal-poor clusters on the $(K, J-K)$ plane.

3. A comparison with [Fe/H] ~ -1.6 near-infrared isochrones, which make different assumptions for [O/Fe], suggests that M13 has an age in the range 14–16 Gyr. This result should be viewed as tentative given uncertainties in our knowledge of stellar evolution (e.g., VandenBerg 1992).

4. The mass function of stars in the mass interval 0.6–0.8 $M_\odot$ is flat near 4 core radii, whereas optical studies at larger radii covering the same mass interval have found a mass function exponent different from zero. Our results are qualitatively consistent with M13 having undergone dynamical evolution.

The authors gratefully acknowledge financial support from the Natural Sciences and Engineering Research Council of Canada (NSERC) and the National Research Council of Canada (NRC). An anonymous referee also provided comments which improved the manuscript.

REFERENCES

Abia, C., & Rebolo, R. 1989, ApJ, 347, 186
Alcaino, G., Liller, W., & Alvarado, F. 1988, ApJ, 330, 569
Armandroff, T. E. 1989, AJ, 97, 375
Arp, H. C. 1955, AJ, 60, 317
Arp, H. C., & Johnson, H. L. 1955, ApJ, 122, 171
Barbuy, B., & Erdelyi-Mendes, M. 1989, A&A, 214, 239
Baum, W. A. 1954, AJ, 59, 422
Baum, W. A., Hiltner, W. A., Johnson, H. L., & Sandage, A. R. 1959, ApJ, 130, 749
Bell, R. A. 1992, MNRAS, 257, 423
Bell, R. A., & Gustafsson, B. 1989, MNRAS, 236, 653
Bergsbusch, P. A., & VandenBerg, D. A. 1992, ApJS, 81, 163
Brown, J. A., Wallerstein, G., & Oke, J. B. 1991, AJ, 101, 1693
Buckley, D. R., & Longmore, A. J. 1992, MNRAS, 257, 731
Casali, M., & Hawarden, T. 1992, JCMT-UKIRT Newsletter, 4, 33
Cohen, J. G. 1978, ApJ, 223, 487
Cohen, J. G., & Frogel, J. A. 1982, ApJ, 255, L39
Cohen, J. G., Frogel, J. A., & Persson, S. E. 1978, ApJ, 222, 165
Davidge, T. J., & Simons, D. A. 1994a, ApJ, 423, 640 (Paper I)
———. 1994b, ApJ, 435, 207 (Paper II)
Djorgovski, S., Piotto, G., & Capaccioli, M. 1993, AJ, 105, 2148
Drukier, G. A., Fahlman, G. G., Richer, H. B., & VandenBerg, D. A. 1988, AJ, 95, 1415
Ferraro, F. R., Fusi Pecci, F., Montegriffo, P., Origlia, L., & Testa, V. 1994, A&A, in press
Folgheraiter, E. L., Penny, A. J., & Griffiths, W. K. 1993, MNRAS, 264, 991
Frogel, J. A., Cohen, J. G., & Persson, S. E. 1983a, ApJ, 275, 773
Frogel, J. A., Persson, S. E., & Cohen, J. G. 1983b, ApJS, 53, 713
Guarnieri, M. D., Dixon, R. I., & Longmore, A. J. 1991, PASP, 103, 675
Kadla, Z. I., Antal, M., Zdarsky, F., & Spasova, N. 1976, Soviet. Astron., 20, 403
Kraft, R. P., Sneden, C., Langer, G. E., & Prosser, C. F. 1992, AJ, 106, 645
Kraft, R. P., Sneden, C., Langer, G. E., & Shetrone, M. D. 1993, AJ, 106, 1490
Laird, J. B., Carney, B. W., & Latham, D. W. 1988, AJ, 95, 1843
Langer, G. E., Suntzeff, N. B., & Kraft, R. P. 1992, PASP, 104, 523
Larson, R. B. 1990, PASP, 102, 709
Lee, Y.-W., Demarque, P., & Zinn, R. 1990, ApJ, 350, 155
Leep, E. M., Wallerstein, G., & Oke, J. B. 1986, AJ, 91, 1117
Leggett, S. K. 1992, ApJS, 82, 351
Lehnert, M. D., Bell, R. A., & Cohen, J. G. 1991, ApJ, 367, 514
Lupton, R. H., & Gunn, J. E. 1986, AJ, 91, 317
Pilachowski, C. A., Wallerstein, G., & Leep, E. M. 1980, ApJ, 236, 508
Pryor, C., Smith, G. H., & McClure, R. D. 1986, AJ, 92, 1358
Reid, N., & Majewski, S. R. 1993, ApJ, 409, 635
Richer, H. B., & Fahlman, G. G. 1986, ApJ, 304, 273

Richer, H. B., Fahlman, G. G., Buonanno, R., & Fusi Pecci, F. 1990, ApJ, 359, L11
Rieke, G. H., & Lebofsky, M. J. 1985, ApJ, 288, 618
Sandage, A. 1970, ApJ, 162, 841
Savedoff, M. P. 1956, AJ, 61, 254
Simons, D. A., Clark, C. C., Massey, S., Smith, S., & Toomey, D. 1993, Proc. SPIE, 1946, 502
Stetson, P. B. 1987, PASP, 99, 191
Stetson, P. B., & Harris, W. E. 1988, AJ, 96, 909
Straniero, O., & Chieffi, A. 1991, ApJS, 76, 525
Suntzeff, N. B. 1981, ApJS, 47, 1
VandenBerg, D. A. 1992, ApJ, 391, 685
VandenBerg, D. A., Bolte, M., & Stetson, P. B. 1990, AJ, 100, 445
VandenBerg, D. A., & Stetson, P. B. 1991, AJ, 102, 1043
Wainscoat, R. J., & Cowie, L. L. 1992, AJ, 103, 332
Wallerstein, G., Leep, E. M., & Oke, J. B. 1987, AJ, 93, 1137
Webbink, R. F. 1985, in IAU Symp. 113, Dynamics of Star Clusters, ed. J. Goodman & P. Hut (Dordrecht: Reidel), 541
Zinn, R., & West, M. J. 1984, ApJS, 55, 45